

GSA Data Repository 2017227

Obelcz et al., 2017, Sub-decadal submarine landslides are important drivers of deltaic sediment flux: Insights from the Mississippi River Delta Front: *Geology*, doi:10.1130/G38688.1.

Supplemental Material

1.1 Geophysical Data acquisition and processing

Table DR1 shows the equipment used in bathymetric data acquisition during 1977-1979, October 2005, February 2009 and June 2014 bathymetric surveys.

Table DR1: Details of bathymetric data acquisition. Reson sonars are multibeam units, Edgetech 4600 is interferometric. ECU = East Carolina University; OSU = Oregon State University; BLM = Bureau of Land Management, USGS = United States Geological Survey; LSU = Louisiana State University; UNO = University of New Orleans; BOEM = Bureau of Ocean Energy Management; SBES=single beam echosounder, GPS= Global Positioning System; CTD = Conductivity, Temperature, and Depth; SVP= Sound Velocity Profiler.

TABLE DR1. PARAMETERS OF BATHYMETRIC DATA ACQUISITION

| Survey | Vessel | Operator | Sonar | Positioning System | Heave/pitch/roll compensation | CTD/SVP | Area (km ²) |
|-------------------------|------------------------------|-------------------------|-------------------|--------------------|-------------------------------|------------------|-------------------------|
| October 1977-March 1979 | Various | BLM, USGS | 110 kHz SBES | Loran C | N/A | N/A | 775 |
| October 2005 | R/V <i>Cape Hatteras</i> | ECU, OSU, USGS | Reson 8101 | Furuno GP-90 | TSS MAHRS | Sea-Bird SBE 9 | 70 |
| February 2009 | R/V <i>Geodetic Surveyor</i> | Fugro Geoservices, Inc. | Reson SeaBat 7125 | Starfix.Nav | Starfix.Nav | Sea-Bird SBE-19 | 30 |
| June 2014 | R/V <i>Coastal Profiler</i> | LSU, UNO, BOEM | Edgetech 4600 | Hemisphere VS111 | SMC IMU-108 | Valeport MiniSVP | 55 |

Bathymetric data from 2005, 2009, and 2014 surveys were processed using Caris Hydrographic Information Processing System and Sidescan Information Processing System. Processing began with automatic filtering (including swath width and depth filters) to remove the majority of bad data. Manual cleaning was then used to further remove spurious data. These datasets were corrected for sound velocity artifacts (utilizing the closest CTD casts in time and space), and tidal corrections and vertical referencing were derived from mean sea level of the NOAA Southwest Pass tidal gauge (station ID 8760959). Digital Elevation Models (DEMs) were then constructed from point clouds using the Combined Uncertainty and Bathymetry Estimator

(CUBE) algorithm (Fig. DR1). DEMs were exported from Caris and imported into ESRI ArcGIS for analysis and interpretation. All morphometric analyses (cross sections, measurements, surface differencing) were done in ArcGIS. Two DoDs were produced, 2014-2009 and 2009-2005 (Fig. 2). The DoD shown in Fig. 2 was regridded using Kriging interpolation method to 25 m² cell size using Golden Surfer. The 1977-1979 data was received as a digitized version of the original hand-contoured maps; the raster was gridded to 100 m² resolution.

1.2 Volumetric calculations

The overall goal of the volumetric calculations was to assess the magnitude of major hurricane-induced failures to failures that occurred without major hurricane forcing. In order to calculate volumetric changes between surveys, the ESRI ArcGIS Cut Fill tool was used (ESRI, 2016). No single gully/lobe complex was covered by all three bathymetric datasets used in volumetric calculations (1977-1979, 2005, 2009, Fig. 1), so several approximations and assumptions had to be made to obtain meaningful comparisons. These assumptions create large uncertainties (discussed in detail in the next section), so the volumetric calculations are only intended to provide an order of magnitude sense of comparison. The volumetric changes are presented in Table DR2 below:

TABLE DR2. MISSISSIPPI RIVER DELTA FRONT VOLUMETRIC CHANGES

| Time Interval | Subset of Study Area | Area (10 ⁶ m ²) | Bulk Volumetric Change (10 ⁶ m ³) | Net Volumetric Change (10 ⁶ m ³) | Uncertainty (+/- 10 ⁶ m ³) | Annual Volume Transported (10 ⁶ m ³ /y ⁻¹) |
|-------------------------|----------------------|--|--|---|---|--|
| March 1979-October 2005 | Mudflow Lobes | 6.8 | 16 | 28 | 3.8 | 1.1 ± 0.15 |

| | | | | | | |
|--------------------------------------|--------------------|-----|-----|-----|-----|------------|
| October 2005- February 2009 | Mudflow Gullies | 6.3 | 5.5 | 2.2 | 3.2 | 0.55 ± 0.8 |
|--------------------------------------|--------------------|-----|-----|-----|-----|------------|

To focus on major storm-driven changes as exclusively as possible, volumetric calculations were done for the 1979-2005 time interval on the mudflow lobe area only (Fig. DR2). The lobe area was defined and digitized on the 2005 Walsh DEM using several criteria, including 1) a positive relief above the surrounding seafloor demarcated by a sharp gradient (5-30°), 2) a hummocky surficial appearance, 3) location directly downslope of mudflow gully(s). The rationale for choosing the mudflow lobe zone to document major hurricane-induced failure is based on two observations: previous authors (including Bea et al. (1983) and Hitchcock et al. (1996)) have noted that major hurricane passage triggers large-scale (<1 km) downslope movement of mudflow lobes, and our assessment that the mudflow lobes are relatively laterally immobile during the 10-year quiescent observation period (Fig. DR3). It is inevitably oversimplifying to assume all movement observed in the lobe zone is hurricane-induced, but volumetric changes in the form of mudflow lobe nose downslope movement are likely to be hurricane-driven changes. The mudflow lobes were assumed to be purely depositional systems, so only volume gains were calculated.

It is probably not a valid assumption to assume that the entire study area has remained static outside the gully/lobe zones. In order to account for change that had occurred throughout the entire study area, a small (0.05 km²) area of the prodelta (pink polygons in Fig. DR1) presumably outside the reach of gully/lobe activity was also assessed for changes using surface differencing, and found to have undergone an average of 1.51 m of erosion between the 1979 and

2005 surveys. This means that the lobe accretion estimates are conservative (bulk volumetric change in Table DR2), assuming the erosion observed in the prodelta reference area is representative of the entire survey area. If the volume lost by regional erosion is added to the accretion estimates in a simple manner (average erosion of reference area multiplied by surface area of lobes), the volume accreted across the mudflow lobe area increases from $1.6 \times 10^7 \text{ m}^3$ to $2.8 \times 10^7 \text{ m}^3$ (net volumetric change in Table DR2).

The same area used for volumetric analysis of the 1979-2005 period could not be used for the 2005-2009 period, because of insufficient survey overlap of the mudflow lobe zones (Fig. 1). Therefore, changes were calculated in the gullies instead; the extent of the gullies was digitized in a manner similar to that described above for the lobes, but negative relief was used for discrimination criteria instead of positive relief. Since the assumption was made that mudflow lobes are purely depositional areas, only negative volumetric changes were tallied for the gullies, simplifying to assume they are purely erosional systems. The total area of the gully zone used in the 2005-2009 calculations and the lobe zone used in the 1979-2005 calculations was approximately equal (both $\sim 6.5 \times 10^6 \text{ m}^2$). There were also changes in the reference area in between 2005 and 2009; the mean vertical change was 0.3 m depth increase, which means the volume of material eroded from the gullies is a maximum estimate. When the “ambient” vertical change is accounted for, the volume of sediment removed from the gullies between 2005 and 2009 drops to $2.2 \times 10^6 \text{ m}^3$.

To put these numbers into a sediment budget context, the volumetric estimates were compared with the total suspended load discharge out of Southwest Pass, as calculated by Allison et al. (2012). The bed (sand) load was disregarded because the majority of it is presumably deposited immediately proximal to the distributary mouth. The suspended load value was expressed as

mass, so to convert to volume a bulk density value (1.5 g/cm^3) derived from gravity and multicores obtained from the study area (Keller et al., 2016) was used. Converting the total suspended load (20.8 million tons/year) to volume yielded an annual volumetric flux of $1.4 \times 10^7 \text{ m}^3/\text{year}$ out of Southwest Pass, which means averaged annually $\sim 8\%$ and $\sim 4\%$ of the suspended sediment that arrives at Southwest Pass is mobilized by mass failures in the survey area during a given “major storm” and “quiescent” year, respectively.

1.3 Estimation of uncertainty

In order to acquire an estimate of uncertainty for the DoDs, the “fixed reference uncertainty” was calculated, following the methods detailed in Schimel et al. (2015). The general premise behind this method is to use a “reference area” that is assumed to be relatively stable between two surveys to acquire a statistical estimate of the DEMs’ vertical uncertainty. A 0.05 km^2 area of the prodelta ($\sim 70 \text{ m}$ water depth, four pink polygons in Fig. DR1) was selected as the reference area because it is downslope of mudflow activity and relatively distant from the sediment plume of Southwest Pass. Values were extracted from the reference area, and statistical parameters were calculated (Fig. DR4). The mean values for the DoDs were within 0.3 m of zero change, validating the assumption that this area remained relatively unchanged between surveys. A 2σ (95% confidence interval for normally distributed data) value was used as the uncertainty range; i.e. values within 2 standard deviations of 0 m were considered within the range of uncertainty and therefore not interpreted as actual change.

A similar method was used for estimation of volumetric uncertainty, with the necessary extra step of scaling into three dimensions. The standard deviation of the reference area was multiplied

by the surface area of the zones (mudflow lobes for 1979-2005, mudflow gullies for 2005-2009), yielding an empirical estimate of volumetric uncertainty.

2.1 Simulation of non-linear waves

To generate and propagate higher order waves (non-linear) on the MRDF, we selected computational fluid dynamics software with built-in capabilities to match requirements specific to our experiments. The FLOW-3D model was selected to perform this analysis, among other available research and commercial codes with varying degrees of strengths and limitations. The FLOW-3D model was selected due to its capability to simulate free-surface flows accurately, using a novel approach, its ability to generate higher order wave theories near the model domain boundaries, and for solving fully three-dimensional flows, without the shallow water approximation.

FLOW-3D is a three dimensional model where fluid motion is described with non-linear transient, second-order differential Navier-Stokes equations. The numerical algorithm used in FLOW-3D is based on both finite difference and finite volume methods applied to a structured computational grid. Structured grids are known for their computational efficiency and ease of discretizing the flow domain. The ability of the model to maintain a sharp interface (air-water) helped retain the non-linear waveform as waves were advancing across the MRDF, and provided for more accurate pressure fields. The finite volume method used in FLOW-3D derives directly from the integral form of the conservation laws for fluid motion, and therefore, retains the conservation properties (FLOW-3D, 2010; Meselhe et al., 2012). FLOW-3D is also capable of capturing the water free-surface accurately, using the so-called true Volume Of Fluid – TrueVOF (Barkudarov, 2004). This approach computes the advection of fluid to all neighboring cells

according to the orientation of the fluid within the cell, and using pressure and velocity boundary conditions it computes the sharp free surface interface. This method is ideal for propagating non-linear waves on the delta front while preserving the non-linear waveform.

The governing equations used in FLOW-3D can be found in (FLOW-3D, 2010). FLOW-3D includes several turbulence closure models, namely Prandtl mixing length, one-equation transport, two-equation k - ϵ transport, Renormalized group theory (RNG), and Large Eddy Simulation (LES) models. The two-equation turbulent closure models are widely used due to their relative computational efficiency and adequate performance for wide range of practical applications (e.g. (Muste et al., 2001)). For the simulations performed here, the Renormalization-Group (RNG) method (Yakhot and Orszag, 1986; Yakhot and Smith, 1992) was used. The RNG model applies statistical methods to the derivation of turbulent kinetic energy and its dissipation rate, and appears to have wider applicability than the standard k - ϵ model when dealing with applications with strong shear regions (e.g., velocity gradients from crest to trough along a waveform).

2.2 Model domain and initial conditions

The computational domain for the model included a 2,000 m long, 5 m wide, and 100 m high rectangular basin. The model resolution was constant (but different) in each x and z dimensions. Horizontal resolution was ~ 0.6 m, vertical resolution ~ 0.25 m, and a time-step of <0.01 s. Model experiments were performed using a flat slope (to eliminate the effect of shoaling) and varied water depths (5-70 m) were instead used to establish pressure differential fields across the study area. All simulations were initialized with a fluid at rest for the required mean fluid depth for each simulation experiment. The fluid density was equal throughout set to seawater density.

To evaluate only the effect of depth and reduce further wave transformations once waves were applied at the boundary, a flat slope bed was selected. This is also a conservative approach, as a sloped delta front would promote shoaling and other forms of dissipation that could render the waves, and thus the seabed pressure differential to be higher. Friction was only applied at the seabed (partial slip) at a value that approximates that of a muddy seabed. Lateral friction was eliminated (full slip) to avoid lateral friction of the waves due to the narrow basin (~5 m).

2.3 Boundary conditions

FLOW-3D possesses the capabilities to simulate regular linear and nonlinear propagating surface waves as well as irregular waves. A linear wave has a sinusoidal surface profile with small amplitude and steepness, while a nonlinear wave has larger amplitude (finite-amplitude), sharper crests and flatter troughs than the linear wave. The nonlinear waves can be categorized into Stokes, cnoidal and solitary waves, according to the wave characters and the mathematical methods used to obtain their solutions (FLOW-3D, 2010). Although the linear wave theory (Airy, 1845) has been used in many applications, the nonlinear wave theories often provide significant improvement in accuracy over the linear wave theory when the wave amplitude is not small. In *FLOW-3D*, three nonlinear wave theories are used for nonlinear wave generation: the fifth-order Stokes wave theory (Fenton, 1985), the Fourier series method for Stokes and cnoidal waves (Fenton, 1999), and McCowan's theory for solitary wave (McCowan, 1891; Munk, 1949). Among them, Fenton's Fourier series method is generally valid for all kinds of periodic propagating waves in deep water, transitional water and shallow water, including linear, Stokes and cnoidal waves, it possesses higher order of accuracy and was the method used for all nonlinear waves in this study. An example of wave propagation is shown in Fig. DR5. Each simulation was run until the entire domain was filled with waves.

2.4 Evaluating pressure change near the seabed

Simulation results were post-processed and visualized using Tecplot360® (Tecplot Inc.). Results included instantaneous three-dimensional velocities, pressures, position of the free-surface, and other hydraulic information such as flow depth and Froude number. At approximately the middle of the model domain, away from boundaries, pressures were extracted at the crest and trough of each wave and were differenced to calculate the pressure change. Wave height, length and period were also extracted to ensure that the wave retained (albeit some frictional dissipation) the wave characteristics applied at the boundary. All simulation results were then plotted against those reported by Henkel (1970). All results (Henkel, 1970) and this study) were converted to SI units (see Fig. 4).

Peak pressure differentials at the seabed ($\Delta p \sim 35$ kPa) in the study area generated by one-year waves ($H_s \sim 6.5$ m; Fig. DR6b) reached similar peak conditions to those produced by hurricane waves (Fig. DR6a), suggesting that movement can be triggered by one-year waves. In depths of 14-50 m one-year waves (~ 6.5 m) produce pressure differentials that exceed those of larger events, such as hurricanes, by more than 15% (Fig. DR6). Failure zones defined by previous studies at various depths and wave loading (grey regions in Fig DR6) do intersect the black solid line (Δp) in Fig DR6a as expected, indicating the failure can occur from these larger hurricane waves. However, it is evident that they are also exceeded at selected locations from forcing from one-year waves (Fig DR6b). The cyclic loading from these higher frequency events may not be as “catastrophic” as that produced by larger events such as hurricanes, but over time, since these events occur annually may trigger failures of similar magnitude.

The selection of flat slope in the model may overestimate wave height and thus pressure, and so can the treatment of a rigid bed. (Bea and Aurora, 1981) reported that a deformable bed could attenuate waves and hence produce lower pressure differentials resulting in lower shear delivered to MRDF sediments. However, even without attenuation (which at these depths is not expected to be large) the results show that pressure differentials simulated here ($\Delta p \sim 7\text{-}35$ kPa) exceed a range of values reported by Henkel (1970) and other authors required to produce failure in the study area (Fig. 4).

3 Gray Literature

Several references are included in this manuscript (project reports, conference proceedings) that may not be available through online research catalogs, but detail findings seminal to our understanding of the Mississippi River Delta Front. This is common since a large amount of the research conducted along this margin was done by hydrocarbon exploration companies, and was therefore not formally published in academic literature. All references included in this manuscript are available in digital format from the corresponding author upon request.

Supplemental References

- Airy, G. B., 1845, Tides and Waves, Encyclopedia Metropolitan.
- Allison, M. A., Demas, C. R., Ebersole, B. A., Kleiss, B. A., Little, C. D., Meselhe, E. A., Powell, N. J., Pratt, T. C., and Vosburg, B. M., 2012, A water and sediment budget for the lower Mississippi–Atchafalaya River in flood years 2008–2010: Implications for sediment discharge to the oceans and coastal restoration in Louisiana: *Journal of Hydrology*, v. 432-433, p. 84-97.
- Barkudarov, M. R., 2004, Lagrangian VOF advection method for FLOW-3D, Flow Science Technical Note #63, Flow Science, Inc.
- Bea, R. G., and Aurora, R. P., 1981, A Simplified Evaluation Of Seafloor Stability, Offshore Technology Conference.
- Bea, R. G., Wright, S. G., Sircar, P., and Niedoroda, A. W., 1983, Wave-induced slides in South Pass Block 70, Mississippi Delta: *Journal of Geotechnical Engineering*, v. 109, no. 4, p. 619-644.
- ESRI, 2016, How Cut Fill works, Volume 2016, Environmental Systems Research Institute.

- Fenton, J. D., 1985, A Fifth-Order Stokes Theory for Steady Waves: *Journal of Waterway Port Coastal and Ocean Engineering-Asce*, v. 111, no. 2.
- , 1999, *Numerical methods for nonlinear waves*, Singapore, World Scientific, *Advances in coastal and ocean engineering*.
- FLOW-3D, 2010, *FLOW-3D Excellence in flow modeling software: Sante Fe, NM 87505*, p. User Manual 9.4 volumes 1 and 2.
- Henkel, D. J., 1970, The role of waves in causing submarine landslides: *Geotechnique*, v. 20, no. 1, p. 75-80.
- Hitchcock, C., Angell, M., Givler, R., and Hooper, J., 1996, A pilot study for regionally-consistent hazard susceptibility mapping of submarine mudslides, offshore Gulf of Mexico.
- Keller, G. P., Bentley, S. J., Georgiou, I. Y., Maloney, J., Miner, M. D., and Xu, K., 2016, Fair-weather versus hurricane-driven sediment dispersal on the Mississippi River Delta Front: insights from sediment-radiochemical measurements: *Geo-Marine Letters*, v. In press, no. In press, p. In press.
- McCowan, J., 1891, On the solitary wave, *Philosophical magazine*, Volume 32, p. 45-58.
- Meselhe, E. A., Georgiou, I., Allison, M. A., and McCorquodale, J. A., 2012, Numerical modeling of hydrodynamics and sediment transport in lower Mississippi at a proposed delta building diversion: *Journal of Hydrology*, v. 472-473, p. 340-354.
- Munk, W. H., 1949, The solitary wave theory and its application to surf problems, *Annals of the New York Academy of Science*, Volume 51, p. 376-423.
- Muste, M., Meselhe, E. A., Weber, L., and Bradley, A. A., 2001, Coupled physical-numerical analysis of flows in natural waterways: *Journal of Hydraulic Research*, v. 39, no. 1.
- Schimmel, A. C. G., Ierodiaconou, D., Hulands, L., and Kennedy, D. M., 2015, Accounting for uncertainty in volumes of seabed change measured with repeat multibeam sonar surveys: *Continental Shelf Research*, v. 111, p. 52-68.
- Yakhot, V., and Orszag, S. A., 1986, Renormalization group analysis of turbulence I. Basic Theory: *Journal of Scientific Computing*, v. 1, p. 1-51.
- Yakhot, V., and Smith, L. M., 1992, The Renormalization Group, the e-Expansion and Derivation of Turbulence Models: *Journal of Scientific Computing*, v. 7, p. 35-61.

Supplemental Figure Captions

Figure DR1 Digital elevation maps generated from October 2005 (A), February 2009 (B) and June 2014 (C) bathymetric surveys, respectively. Color bathymetry data overlays a hill-shaded relief map (azimuth 315° , altitude 45°). Four pink polygons show the areas used to calculate the fixed reference uncertainty.

Figure DR2 Digital elevation map from October 2005 with mudflow gully (blue) and mudflow lobe (red) areas used for volumetric calculations digitized. The extents of Supplemental Figure DR3 are shown as the dashed black box.

Figure DR3 Gradient map of a mudflow lobe showing the relative lack of lateral change between the 2005, 2009, and 2014 surveys. The lack of lateral change stands in contrast to surveys bracketing major hurricanes, where mudflow lobes move hundreds of meters to kilometers downslope.

Figure DR4 Histogram showing distribution of depth change within the fixed reference area for the 2009-2005 DoD. Values are shown as a percent of the total cells included within the reference area (shown as four pink polygons in Fig. DR1). These data are roughly normally distributed around -0.25 m, and 2 times the standard deviation (0.5 m, 95% confidence interval) were chosen as the uncertainty range.

Figure DR5 Example pressure distribution and velocity variation along a non-linear wave using FLOW-3D; the approximate wave at the boundary (left – outside the frame) is $H_s = 6.5$ m, $T = 9$ seconds). At the right boundary, outflow boundary was selected, to radiate the entire wave outside the domain and avoid wave reflections back into the domain.

Figure DR6: Relationship between water depth, wave height (blue) and pressure change (black) on the sea bottom. (A) Modified from (Henkel, 1970) where the author used a sinusoidal pressure change resulting from linear waves to establish the pressure fields across a wavelength, (B) this study, using fully non-linear waves propagated across the delta front on an assumed flat slope and across variable depth. Light grey marks in the figure show regions of potential delta front failure as reported by the listed authors. The evolution of pressure change (black) from

water depths between 5 – 70 m look similar between linear sinusoidal and fully non-linear waves, however, during our study these pressure changes can be achieved with wave heights (blue) that occur more frequently i.e. ~1-year return period.

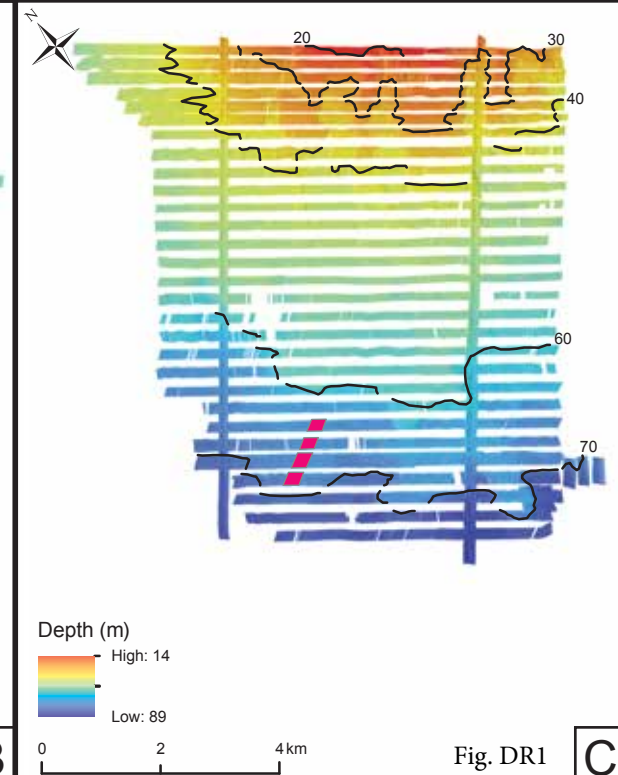
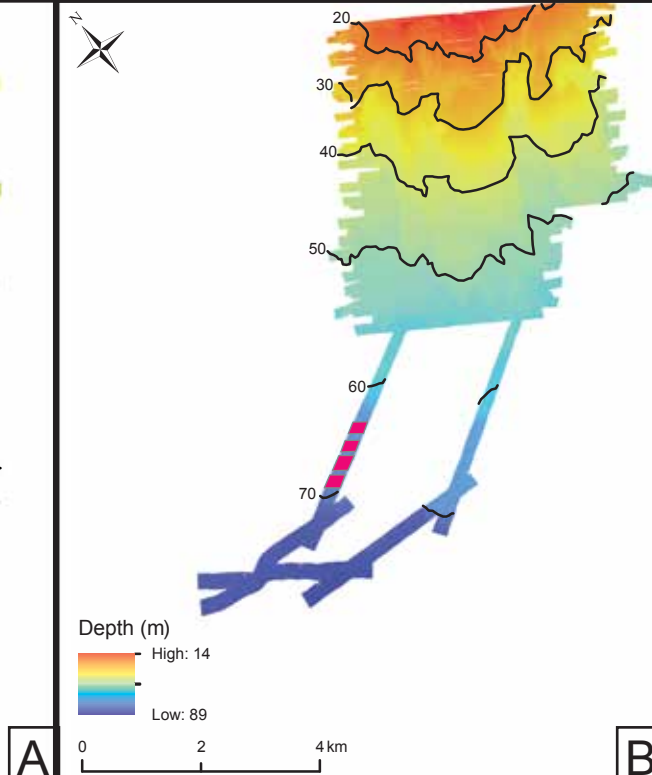
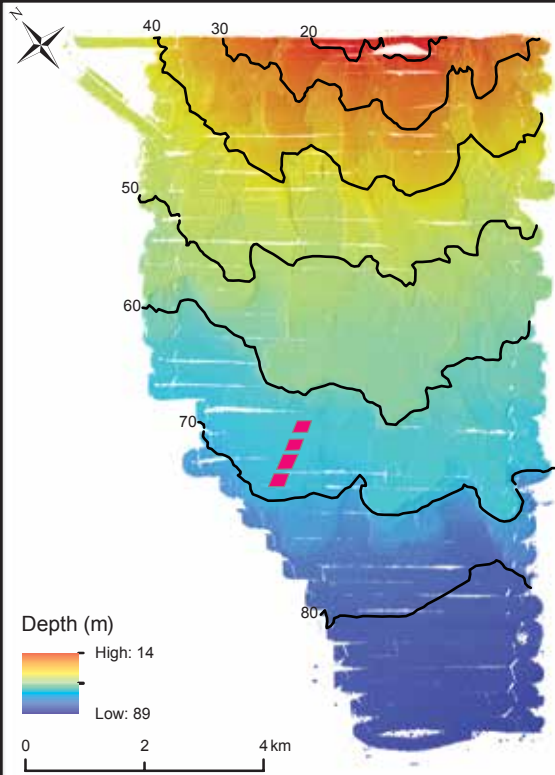
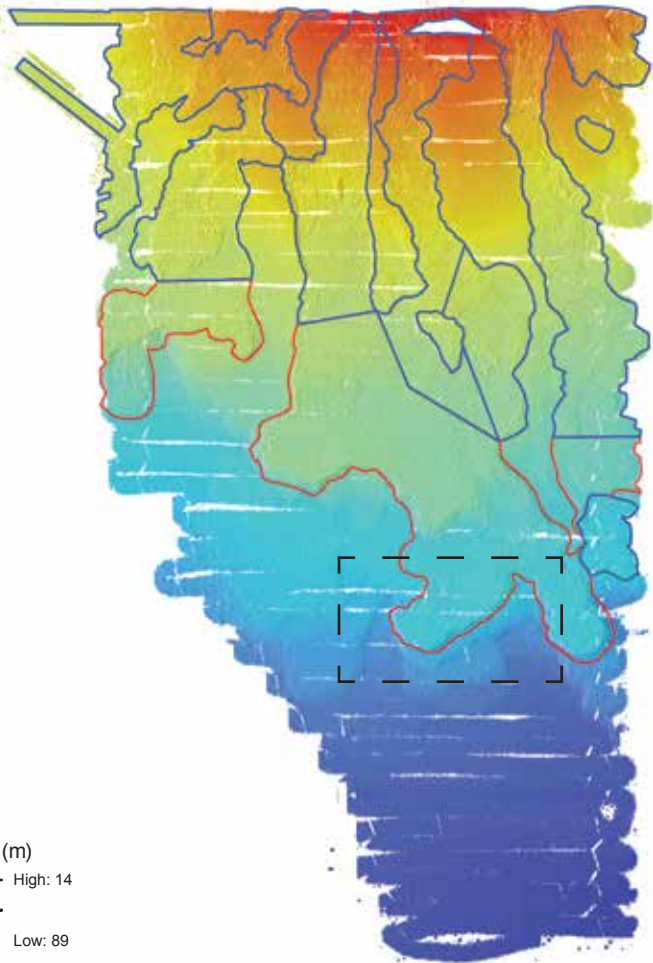


Fig. DR1

C



Depth (m)

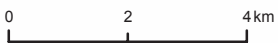
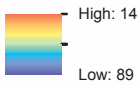
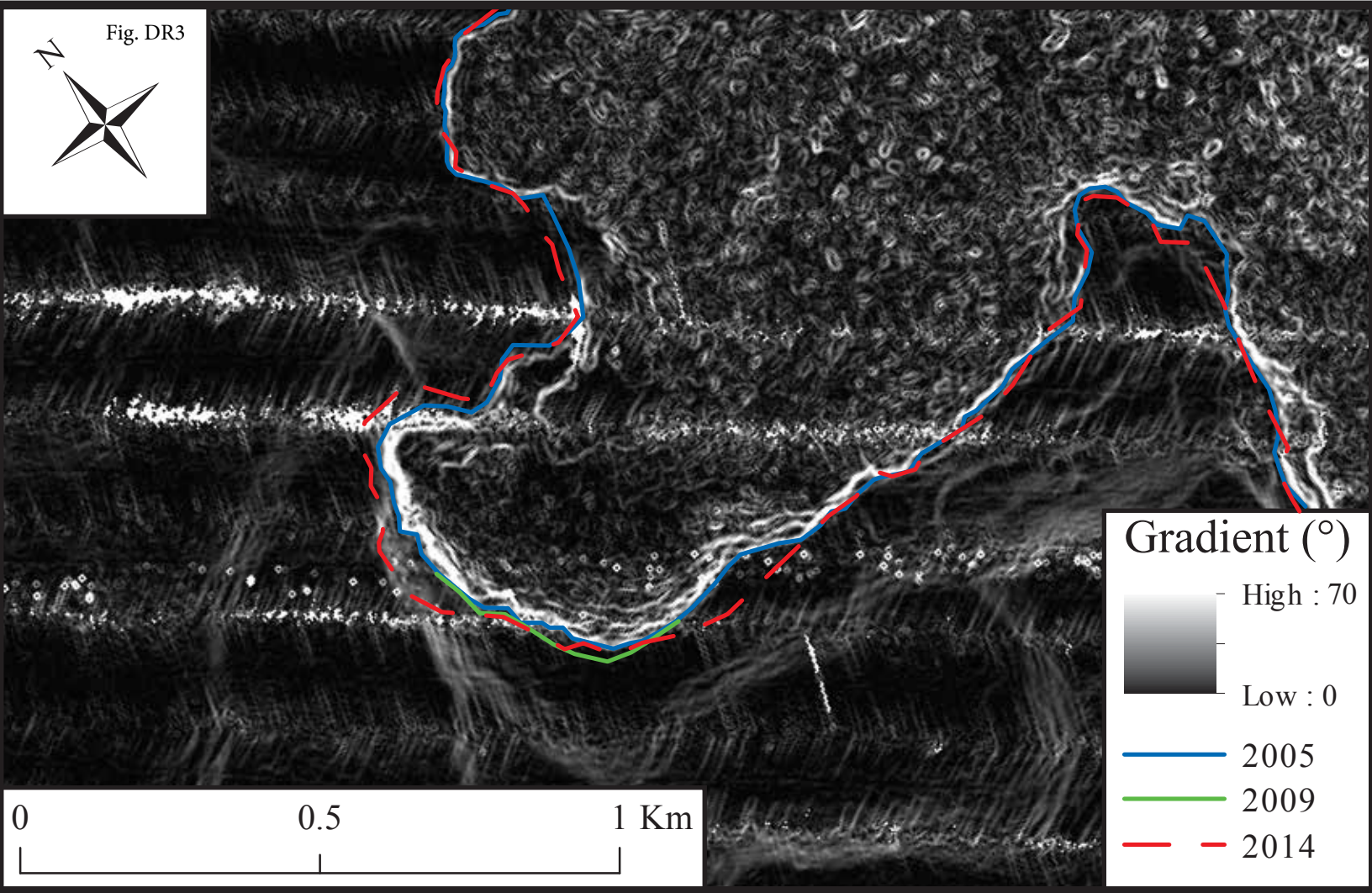
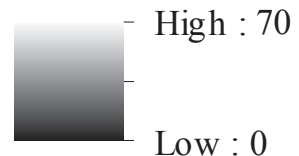


Fig. DR2

Fig. DR3



Gradient ($^{\circ}$)



- 2005
- 2009
- - 2014

0 0.5 1 Km

Vertical uncertainty of 2009 and 2005 Surface Differencing

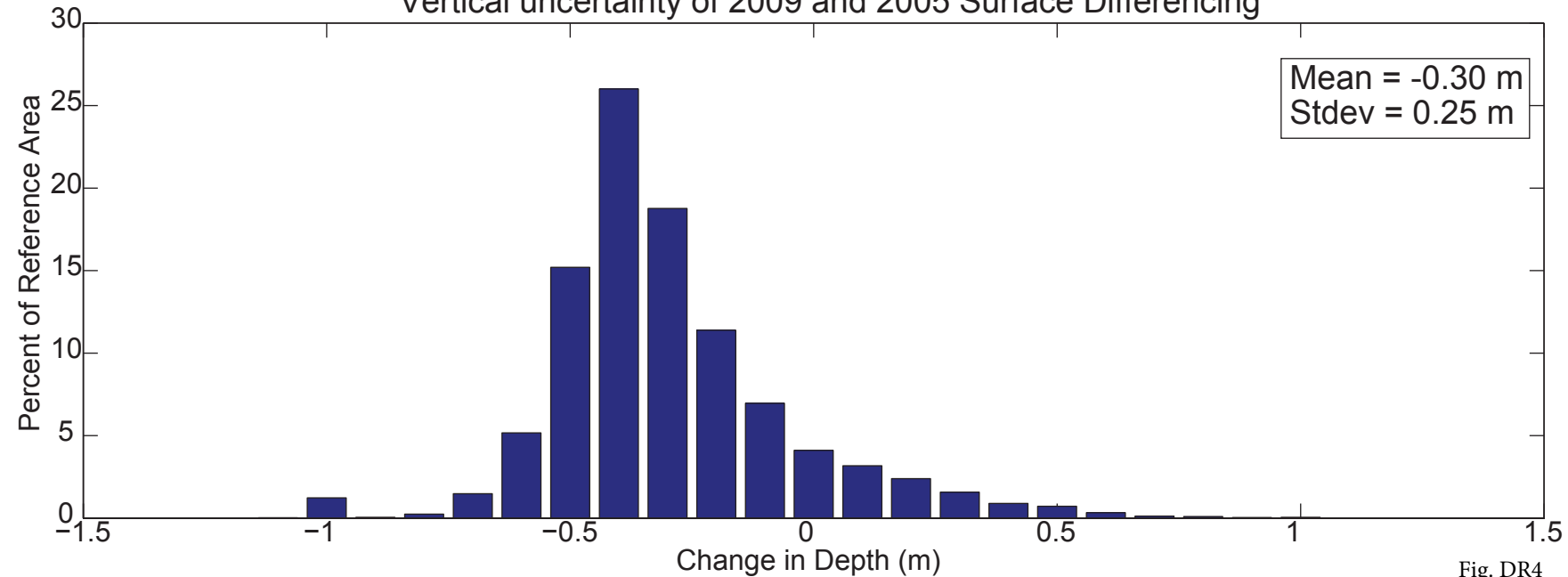


Fig. DR4

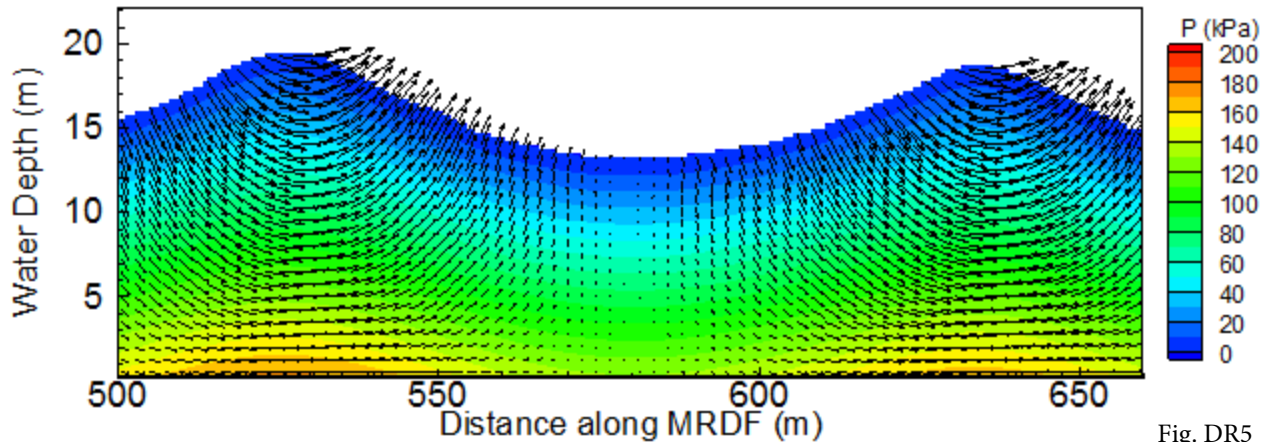


Fig. DR5

